

COMMUNICATION


 Cite this: *RSC Adv.*, 2015, 5, 1808

 Received 11th October 2014
Accepted 28th November 2014

DOI: 10.1039/c4ra12201a

www.rsc.org/advances

A europium–lipoprotein nanocomposite for highly-sensitive MR-fluorescence multimodal imaging†

Qi Wang, Shizhen Chen, Qing Luo, Maili Liu and Xin Zhou*

A novel reconstituted high-density lipoprotein (rHDL) nanocomposite has been prepared for highly-sensitive magnetic resonance (MR)-fluorescence multimodal imaging. Such a nanocomposite is able to enhance the MR sensitivity up to 129 fold in comparison to the traditional small molecule MRI agent based on paramagnetic chemical exchange saturation transfer (PARACEST). It has also demonstrated specific targeting to macrophage cells, which shows great potential for the detection of atherosclerosis.

Protein-nanoparticles have gained importance for biological imaging and drug delivery given their high payloads, improved detection sensitivity, long circulation times and the ease of integration of multiple properties. In respect of the large protein family, lipoprotein-like nanoparticles offer further advantages for biological targeting.¹ Lipoproteins are a family of plasma nanoparticles responsible for the transportation of lipids throughout the body.

High-density lipoprotein (HDL), the smallest of the lipoprotein family, is a complex of lipids (phospholipids, cholesterol, *etc.*) and apolipoproteins with size of 7–13 nm. The HDL carries various apolipoproteins, and the most abundant protein components are apolipoprotein A-I (ApoA-I) and apolipoprotein A-II (ApoA-II). The apolipoprotein reduces the surface pressure on the lipoprotein, thereby stabilizing it. More importantly, the HDL plays the main actor in the process known as reverse cholesterol transportation (RCT), in which the HDL promotes the transportation of excess cholesterol from extra-hepatic or peripheral tissue to the liver for elimination through the biliary system. Reverse efflux of cholesterol from plaque macrophages has an important protective effect in atherosclerosis, and the

HDL is believed to have other atheroprotective properties as well.² In the last decade, reconstituted HDL (rHDL) has been developed to be contrast agent nanocarrier in MRI,^{3,4} CT,⁵ fluorescence,⁶ *etc.* Several multimodal agents were also developed,¹ mainly due to the flexibility of the rHDL to be modified. Moreover, the rHDL processes specificity to macrophages due to the HDL receptor. Because of the link between macrophage density and high-risk atherosclerotic plaque⁷ or other inflammatory diseases,⁸ imaging of macrophage is always an attractive goal.⁹

Paramagnetic chemical exchange saturation transfer (PARACEST) agents are a unique class of magnetic resonance imaging (MRI) contrast agents (CAs) that are currently under intense scrutiny for MR molecular imaging and MR image-guided drug delivery applications. The peculiarity of PARACEST agents is the frequency-encoding mechanism of contrast generation that can be switched on at will by irradiating, with a selective radio frequency (RF) field, the exchangeable water protons of the agent.¹⁰ PARACEST agents hold promise as sensors for measuring various parameters of their biological environment, such as pH,¹¹ temperature,¹² metabolite¹³ or metal ion concentration.¹⁴ PARACEST probes are ideally suited for molecular imaging since, as opposed to gadolinium based MRI agents, the contrast can be switched on and off at will. They cause paramagnetically shifted mobile protons in slow exchange with bulk water. The irradiation of these protons affects the magnetic resonance signal of water protons through the chemical exchange. PARACEST agents have strong potential to improve the specificity of MRI diagnoses. For instance, the chemical exchange of amide protons is base-catalyzed and therefore PARACEST agents with amides can be used to measure pH and detect tumor acidosis,¹⁵ which may improve specificity for detecting tumors relative to normal tissues.

Unfortunately, the Achilles' heel of PARACEST agents is its relatively modest sensitivity. Typically millimolar concentrations of the agent are required,¹⁶ and the PARACEST detection of target molecules is not possible at low concentration. To improve the detection sensitivity, PARACEST agents have been

Key Laboratory of Magnetic Resonance in Biological Systems, State Key Laboratory for Magnetic Resonance and Atomic and Molecular Physics, National Center for Magnetic Resonance in Wuhan, Wuhan Institute of Physics and Mathematics, Chinese Academy of Sciences, Wuhan 430071, China. E-mail: xinzhou@wipm.ac.cn

† Electronic supplementary information (ESI) available: Preparation and characterization of rHDLs; methods of cell culture, CEST MRI experiments and cellular fluorescence imaging. See DOI: 10.1039/c4ra12201a

conjugated to nanocarriers such as dendrimers,¹⁷ linear polymers,¹⁸ liposomes¹⁹ and other nano carriers^{20–22} to increase the number of exchangeable sites per agent. We took rHDL in consideration as a PARACEST agent candidate mainly because one particle contains hundreds of lipids, which can be substituted by PARACEST active lipid, and thus the exchangeable sites are able to be increased.

Multimodal imaging has emerged as a novel concept that combines different imaging methodologies to provide complementary information in biological studies and medical diagnostics. Optimally, multimodal probes integrate, within the same molecular entity, reporters for each of the techniques, enabling the visualization of identical biodistribution.²³ Furthermore, a multimodal contrast agent can be designed to exploit the strengths of two complimentary imaging modalities, which can multiply the value of the agent for biomedical imaging. MRI is often used for presurgical planning to identify the macroscopic features of pathological tissues, and fluorescence imaging is emerging as a useful intrasurgical tool to identify microscopic margins of pathological tissues.²⁴ Therefore, conjugating fluorescent agents and PARACEST agents to rHDL nanoparticles would be a synergistic approach.

Here we designed and prepared a high-payload PARACEST and fluorescence dual-modal contrast agent based on rHDL. The PARACEST MR-fluorescence rHDL was prepared *via* a self-assembly process.^{25,26} To make rHDL PARACEST active, a phospholipid linked with Eu-DOTA derivant was synthesized and introduced in the particle. A phospholipid linked with rhodamine was also introduced to achieve fluorescence imaging (Fig. 1). After that, we used a cell model to verify the specificity of rHDL for atherosclerotic plaques, and fluorescence imaging was conducted to confirm the cell intake of the rHDL. The high-payload of PARACEST agents can improve the CEST detection sensitivity. Therefore, the development of a high-payload, dual-modality MRI contrast agent would have good

utility for the detection of atherosclerotic plaques, and may improve treatment planning.

The rHDL was prepared following the well-established protocols.^{25,26} This method is based on the self-assembly of lipid and apolipoprotein. In this case, ApoA-I apolipoprotein was used. PARACEST phospholipid Eu-DOTA-3AmCE-DMPE, fluorescent phospholipid Rhod-DMPE and DPPC were mixed and dissolved in PBS within cholate sodium. Then, the solution was incubated with ApoA-I in 37 °C for 12 h. After dialysis to PBS, Eu-labeled fluorescent rHDL (Eu-Rhod-rHDL) was produced and subsequently characterized. Control group rHDL (Rhod-rHDL) was prepared similarly except Eu-DOTA-3AmCE-DMPE was substituted by equivalent DMPE (see ESI† for details).

The mean size of Eu-Rhod-rHDL determined by the DLS was 14.3 nm in aqueous solution, which was a little larger than the size of Rhod-rHDL of 8.8 nm. It results from the increase of occupied space of Eu labeled phospholipid Eu-DOTA-3AmCE-DMPE than DMPE (see ESI, Fig. S3a†). The polydispersity index (PDI) of Eu-Rhod-rHDL and Rhod-rHDL are 0.268 and 0.194, relatively. The increase of PDI of Eu-Rhod-rHDL is mainly because of the introducing of Eu-labeled phospholipid. The result of TEM confirmed that the Eu-Rhod-rHDL had a size of ~10 nm and relatively uniform diameter distribution (see ESI, Fig. S3b†). Still, the size of Eu-Rhod-rHDL and Rhod-rHDL are both among the typical size range of previously reported rHDLs.⁴ The zeta potential of Eu-Rhod-rHDL and Rhod-rHDL were -2.8 mV and -23 mV, respectively, due to the introducing of Eu(III) chelate.

Investing the fluorescence properties of rHDLs, the conjugation of rhodamine to rHDL shifted the emission wavelength by 12 nm, relative to the corresponding bands for the free dye. When Eu(III) labeled phospholipid was introduced, a 70 nm red shift was observed in the Eu-Rhod-rHDL (see ESI, Fig. S3c†). However, quenching was not observed from the rhodamine in Eu-Rhod-rHDL compared with the free dye. This verified that it is negligible of the potential fluorescence quenching generated by Eu(III).

The number of Eu(III) per Eu-Rhod-rHDL particle was ~155, which was determined by the ratio of the concentration of Eu(III) and ApoA-I. The concentration of Eu(III) was obtained by ICP-AES. Generally, the traditional single molecular PARACEST agent required a working concentration of at least 10 mM to produce notable CEST effect.¹⁶ By using rHDL as a carrier, the working concentration of PARACEST agent was expected to be reduced two orders of magnitude, down to sub millimolar level compared with traditional agents.

The atherosclerosis develops from the macrophages entering the artery wall and natural high-density lipoprotein can target the macrophages due to the HDL receptor. Thus, macrophages can be used as a model to testify the specificity of atherosclerosis agents. The ApoA-I protein on the Eu-Rhod-rHDL particle could also play a dominant role in facilitating receptor-mediated endocytosis. To evaluate the efficiency and specific cellular uptake for the Eu-Rhod-rHDL, murine macrophage RAW 264.7 cells were incubated in 20 µg mL⁻¹ Eu-Rhod-rHDL solution for 4 h, and normal cells WI-38 were processed under

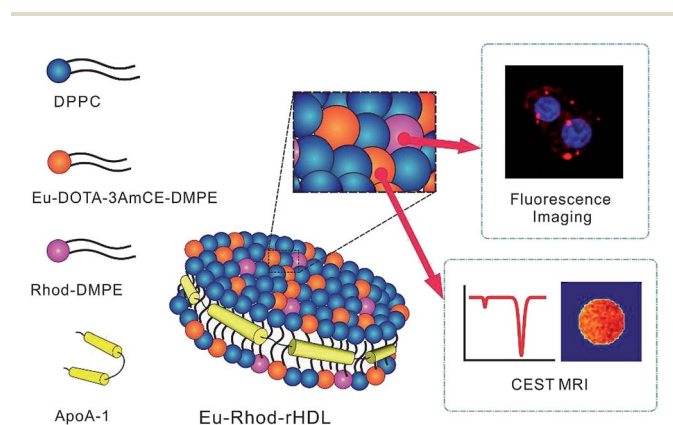


Fig. 1 The scheme of preparation and functioning of dual-modal contrast agent, Eu-Rhod-rHDL. The dual-modal rHDL was prepared *via* a self-assembly process. The Eu-DOTA-3AmCE-DMPE produced the CEST effect of MRI, while fluorescence imaging was achieved due to Rhod-DMPE. The Eu-Rhod-rHDL enhanced the PARACEST detection sensitivity up to 129 folds compared to the conventional small molecular agent, and it could specifically image macrophages.

the same procedure. Afterwards the nuclei were stained by DAPI (blue). Then the intake of the macrophage was investigated by the laser scanning confocal microscopy (Fig. 2). In the confocal photographs, the Eu-Rhod-rHDL, represented by red color indicated by the rhodamine on the particle, can be clearly observed in the cytoplasm in the macrophages, while almost none observed of the normal cells. These results clarified that more Eu-Rhod-rHDL entered macrophages in the incubation process, while little entered the normal cells. Therefore, the specificity of Eu-Rhod-rHDL to macrophages like natural high-density lipoproteins was verified, and further demonstrated that the Eu-Rhod-rHDL could be treated as a contrast agent for atherosclerosis.

The chemical exchange saturation transfer property of the agent was investigated by acquiring CEST Z-spectra on a 500 MHz NMR spectrometer at 298 K (Fig. 3a), and 9% CEST effect was observed at the concentration of 77.4 μM for the Eu-Rhod-rHDL. This CEST effect was generated from the bound water on the Eu(III) chelate. When deployed a selective saturation pulse at the frequency of bound water, the signal of bulk water decreased due to the chemical exchange with bound water. Thus the signal of bound water was amplified and bound water was detected indirectly. The exchange site of bound water was found at +49 ppm, which is agreeable to previous small molecule Eu(III) PARACEST agents of ~ 50 ppm reported before.²⁷

The comparison of CEST performance of different CEST agents was shown in Fig. 3b. Eu-DOTA-4AmCE is a small molecule PARACEST agent with four AmCE groups conjugated to -COOH of DOTA,⁶ which is similar to Eu(III) labeled phospholipid Eu-DOTA-3AmCE-DMPE with three AmCE groups. CEST Z-spectrum of Eu-DOTA-4AmCE with concentration of 10 mM for Eu(III) was conducted in the same acquisition condition relative to the Eu-Rhod-rHDL, and 9% CEST effect was observed. Same CEST effects were observed in the Eu-Rhod-rHDL with similar concentration for Eu(III) (12 mM) while no CEST effect was found in rHDL, which confirms that the Eu-Rhod-rHDL has almost the same CEST performance. Accordingly, the sensitivity was improved in about 129 folds (on per particle basis) with 155 Eu-labeled phospholipids on the

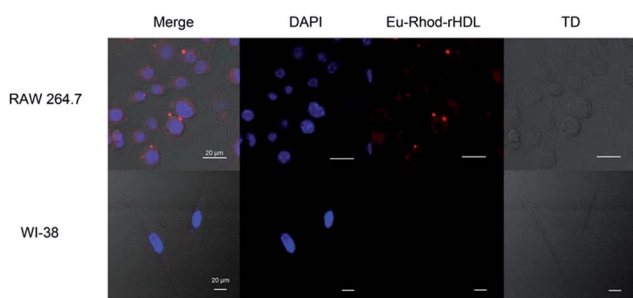


Fig. 2 The laser scanning confocal microscopy photographs of RAW 264.7 and WI-38 cells. Murine macrophage RAW 264.7 and normal human fetal lung fibroblast WI-38 cells were incubated in 20 $\mu\text{g mL}^{-1}$ Eu-Rhod-rHDL solution for 4 h. Cells were stained with DAPI (blue) to show the nuclei and Eu-Rhod-rHDL was shown in red. The microscopy photographs demonstrated that the Eu-Rhod-rHDL was able to enter macrophages specifically. The scale bar represents 20 μm .

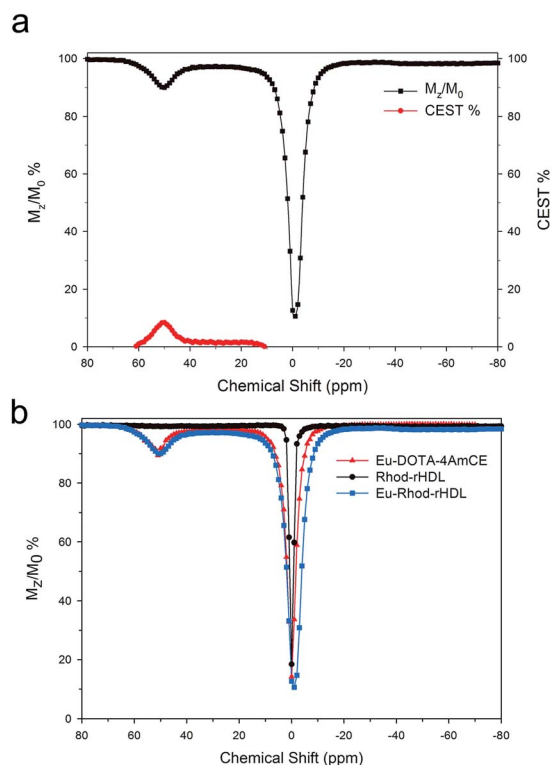


Fig. 3 The chemical exchange saturation transfer effect of Eu-Rhod-rHDL. (a) The CEST spectrum of Eu-Rhod-rHDL at the concentration of 77.4 μM for Eu-Rhod-rHDL generated a CEST effect at +49 ppm, and the CEST% was 9%. (b) The CEST spectra of comparison between Eu-Rhod-rHDL, Rhod-rHDL and small molecule PARACEST agents Eu-DOTA-4AmCE. The concentration of Eu-Rhod-rHDL, Rhod-rHDL and Eu-DOTA-4AmCE were 77.4 μM , 80 μM and 10 mM, respectively. Eu-Rhod-rHDL and Eu-DOTA-4AmCE generated similar CEST effect, which demonstrated that our developed nanocomposite is able to enhance the MR sensitivity up to 129 folds in comparison to the traditional small molecule PARACEST agent.

Eu-Rhod-rHDL. This presents that the CEST effect almost scaled with the concentration of the Eu(III), while small decrement of the CEST effect may be caused by the diminishment of the exchange rate of bound water in the nano structure of the Eu-Rhod-rHDL.

In order to get further understanding of the CEST property of the Eu-Rhod-rHDL, the CEST MRI (Fig. 4) was conducted. With a saturation pulse of 8 μT at +50 ppm for 5 s, the Eu-Rhod-rHDL sample with the concentration of 77.4 μM generated a mean 8% CEST effect. To produce the equivalent CEST effect ($\sim 8\%$) in the cell pellet imaging, the concentration of Eu-Rhod-rHDL in the macrophages should be at least 77.4 μM . Based on the macrophage's volume and the number of Eu(III) per Eu-Rhod-rHDL, the amount of the nanocomposites per macrophage required for the pellet CEST imaging is about 1.9×10^8 particles. Compared with the acquisition condition of the CEST spectra above, the images with lower saturation pulse showed the similar CEST property, and no obvious decrement of the CEST effect was observed. The elevation of sensitivity expanded the range of use of PARACEST agents compared to traditional ones, and macrophages can be probed using the

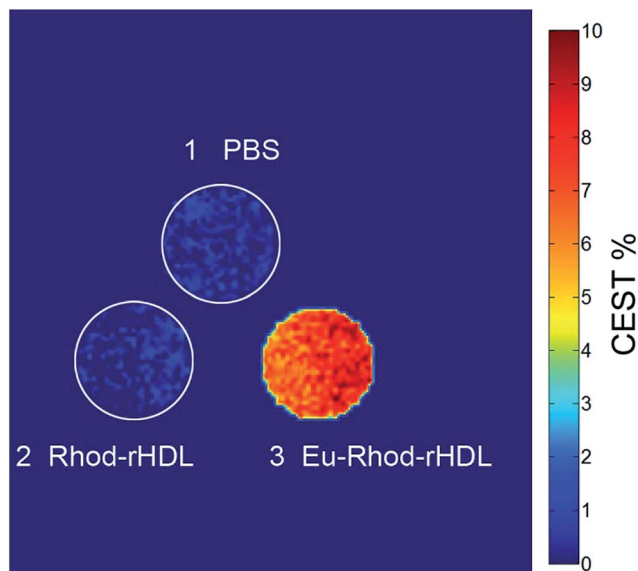


Fig. 4 Chemical exchange saturation transfer MRI of (1) PBS at pH 7.4, (2) Rhod-rHDL with a concentration of 80 μM and (3) Eu-Rhod-rHDL with a concentration of 77.4 μM . TR/TE = 5012 ms/6 ms, 128 \times 128 matrix, FOV 20 \times 20 mm², saturation pulse 8 μM at +50 ppm for 5 s.

Eu-Rhod-rHDL. Furthermore, this agent showed potential in the application of the detection of atherosclerotic plaques *in vivo*.

Conclusions

In conclusion, we have developed a dual-modality imaging contrast agent that used the rHDL platform to carry a PARACEST agent and a fluorescent tag. The Eu-Rhod-rHDL was shown a 129 folds sensitivity enhancement of the CEST effect in comparison to the conventional small molecule PARACEST agent, which is crucial for the detection of low concentration molecular markers in MRI-based molecular imaging studies. The phospholipids on the surface of the nanoparticles provide broad flexibility to the rHDL platform, and it can be exploited not only for MRI but also for fluorescence imaging. More importantly, the rHDL nanoparticles specific uptake by macrophages shows great potential in the detection of atherosclerosis using such nanocomposite.

Acknowledgements

This work was supported by the Natural Science Foundation of China (81227902, 21305156, 21221064 and 21120102038) and the Chinese Academy of Sciences (KJCX2-EW-N06-04).

Notes and references

- 1 D. P. Cormode, T. Skajaa, M. M. van Schooneveld, R. Koole, P. Jarzyna, M. E. Lobatto, C. Calcagno, A. Barazza, R. E. Gordon, P. Zanzonico, E. A. Fisher, Z. A. Fayad and W. J. Mulder, *Nano Lett.*, 2008, **8**, 3715–3723.
- 2 A. J. Lusis, *Nature*, 2000, **407**, 233–241.

- 3 J. C. Frias, K. J. Williams, E. A. Fisher and Z. A. Fayad, *J. Am. Chem. Soc.*, 2004, **126**, 16316–16317.
- 4 J. C. Frias, Y. Ma, K. J. Williams, Z. A. Fayad and E. A. Fisher, *Nano Lett.*, 2006, **6**, 2220–2224.
- 5 A. Shaish, G. Keren, P. Chouraqui, H. Levkovitz and D. Harats, *Pathobiology*, 2001, **69**, 225–229.
- 6 D. P. Cormode, K. C. Briley-Saebo, W. J. Mulder, J. G. Aguinaldo, A. Barazza, Y. Ma, E. A. Fisher and Z. A. Fayad, *Small*, 2008, **4**, 1437–1444.
- 7 K. J. Moore and I. Tabas, *Cell*, 2011, **145**, 341–355.
- 8 E. F. Morand, M. Leech and B. Jurgen, *Nat. Rev. Drug Discovery*, 2006, **5**, 399–410.
- 9 J. Sanz and Z. A. Fayad, *Nature*, 2008, **451**, 953–957.
- 10 S. Zhang, P. Winter, K. Wu and A. D. Sherry, *J. Am. Chem. Soc.*, 2001, **123**, 1517–1518.
- 11 N. McVicar, A. X. Li, M. Suchy, R. H. Hudson, R. S. Menon and R. Bartha, *Magn. Reson. Med.*, 2013, **70**, 1016–1025.
- 12 S. Zhang, C. R. Malloy and A. D. Sherry, *J. Am. Chem. Soc.*, 2005, **127**, 17572–17573.
- 13 D. V. Hingorani, E. A. Randtke and M. D. Pagel, *J. Am. Chem. Soc.*, 2013, **135**, 6396–6398.
- 14 R. Trokowski, J. M. Ren, F. K. Kalman and A. D. Sherry, *Angew. Chem., Int. Ed.*, 2005, **44**, 6920–6923.
- 15 Y. Wu, T. C. Soesbe, G. E. Kiefer, P. Zhao and A. D. Sherry, *J. Am. Chem. Soc.*, 2010, **132**, 14002–14003.
- 16 T. Mani, G. Tircso, O. Togao, P. Zhao, T. C. Soesbe, M. Takahashi and A. D. Sherry, *Contrast Media Mol. Imaging*, 2009, **4**, 183–191.
- 17 M. M. Ali, M. P. Bhuiyan, B. Janic, N. R. Varma, T. Mikkelsen, J. R. Ewing, R. A. Knight, M. D. Pagel and A. S. Arbab, *Nanomedicine*, 2012, **7**, 1827–1837.
- 18 Y. Wu, Y. Zhou, O. Ouari, M. Woods, P. Zhao, T. C. Soesbe, G. E. Kiefer and A. D. Sherry, *J. Am. Chem. Soc.*, 2008, **130**, 13854–13855.
- 19 S. Aime, D. Delli Castelli and E. Terreno, *Angew. Chem., Int. Ed.*, 2005, **44**, 5513–5515.
- 20 G. Ferrauto, F. Carniato, L. Tei, H. Hu, S. Aime and M. Botta, *Nanoscale*, 2014, **6**, 9604–9607.
- 21 P. M. Winter, K. Cai, J. Chen, C. R. Adair, G. E. Kiefer, P. S. Athey, P. J. Gaffney, C. E. Buff, J. D. Robertson, S. D. Caruthers, S. A. Wickline and G. M. Lanza, *Magn. Reson. Med.*, 2006, **56**, 1384–1388.
- 22 G. Liu, M. Moake, Y. E. Har-el, C. M. Long, K. W. Chan, A. Cardona, M. Jamil, P. Walczak, A. A. Gilad, G. Sgouros, P. C. van Zijl, J. W. Bulte and M. T. McMahon, *Magn. Reson. Med.*, 2012, **67**, 1106–1113.
- 23 J. Li and J. J. Zhu, *Analyst*, 2013, **138**, 2506–2515.
- 24 S. H. Tang, J. Wang, C. X. Yang, L. X. Dong, D. Kong and X. P. Yan, *Nanoscale*, 2014, **6**, 8037–8044.
- 25 A. Jonas, *Methods Enzymol.*, 1986, **128**, 553–582.
- 26 P. C. Rensen, R. L. de Vruhe, J. Kuiper, M. K. Bijsterbosch, E. A. Biessen and T. J. van Berkel, *Adv. Drug Delivery Rev.*, 2001, **47**, 251–276.
- 27 S. Viswanathan, S. J. Ratnakar, K. N. Green, Z. Kovacs, L. M. De Leon-Rodriguez and A. D. Sherry, *Angew. Chem., Int. Ed.*, 2009, **48**, 9330–9333.